


Article

Mechanisms of Charged Particle Motion during Capture by Charged Droplets in Marine Diesel Exhaust

Lin Yang^{1,2}, Peilin Zhou¹, Haibin Wang¹ , Ning Mei^{2,3,*} and Han Yuan^{2,*} 

¹ Department of Naval Architecture, Ocean & Marine Engineering, University of Strathclyde, Glasgow G4 0LZ, UK; lin.yang@strath.ac.uk (L.Y.); peilin.zhou@strath.ac.uk (P.Z.); haibin.wang@strath.ac.uk (H.W.)

² College of Engineering, Ocean University of China, Qingdao 266100, China

³ College of Mechanical & Electrical Engineering, Qingdao City University, Qingdao 266100, China

* Correspondence: nmei@ouc.edu.cn (N.M.); hanyuan@ouc.edu.cn (H.Y.)

Abstract: Marine diesel engine emissions of particulate matter pose a significant threat to the environment and human health, necessitating the development of new technologies for their reduction. Among all of these clean and sustainable methods, electrohydrodynamic methods, particularly the use of charged droplets in a wet electrostatic scrubber, offer a viable solution for effectively eliminating particulate matter. This study investigates the basic mechanism of wet electrostatic scrubbers, which involves spraying charged droplets to capture small-sized particles and applying electrostatic forces to act on the oppositely charged particles. In this paper, a mathematical model is presented to describe the process of particle motion when being captured by droplets under the effect of an electrostatic field. Additionally, a co-simulation with ANSYS Fluent and MATLAB is conducted to simulate this process. The mathematical calculation results and co-simulation results are basically consistent, and the average error between these two results is 1.5%. Then, the effect of features, such as electrostatic field strength, particle size, and droplet size, on the particle capture process is analyzed. This study mainly discusses the relationship between the electrostatic field, gas flow field, and particle motion and proposed a theoretical model and numerical simulation method to describe this mechanism relationship. The research findings provide important evidence for the efficient control of ship pollutants, which is of significant importance for the sustainable development of the international shipping industry.

Keywords: particulate matter emission; wet electrostatic scrubber; capture mechanism; co-simulation



Citation: Yang, L.; Zhou, P.; Wang, H.; Mei, N.; Yuan, H. Mechanisms of Charged Particle Motion during Capture by Charged Droplets in Marine Diesel Exhaust. *Sustainability* **2024**, *16*, 7354. <https://doi.org/10.3390/su16177354>

Academic Editors: José Carlos Magalhães Pires and Marc A. Rosen

Received: 4 June 2024

Revised: 12 August 2024

Accepted: 14 August 2024

Published: 27 August 2024



Copyright: © 2024 by the authors. Licensee MDPI, Basel, Switzerland. This article is an open access article distributed under the terms and conditions of the Creative Commons Attribution (CC BY) license (<https://creativecommons.org/licenses/by/4.0/>).

1. Introduction

Against the backdrop of contemporary economic globalization, approximately 85% of global trading shipments utilize maritime routes, of which nearly 70% are concentrated within a distance of 400 km from the coastline [1–4]. The current state of marine conditions reveals that the emissions of marine diesel engines cause serious pollution to both the air and ocean environments. Shipping emissions have a significant impact on air quality far from the source, and some pollutants disperse globally, leading to effects on the climate as well [5–7]. The emissions of particulate matter (PM) from marine transport are highly associated with adverse human health outcomes. Studies have estimated that these emissions are responsible for 60,000 cardiopulmonary and lung cancer deaths every year worldwide, with a majority of fatalities occurring in coastal areas near major ports. More recent estimates indicate that this figure has increased to 87,000 deaths per year globally [8–10]. The exhaust gas discharged by marine diesel engines contains various pollutants, including sulfur dioxide (SO₂), nitrogen oxide (NO_x), and PM [11–17]. Unlike SO₂ and NO_x, there are hardly appropriate regulations for the emission of PM from marine diesel engines due to insufficient technology. The difficulty in developing accurate and reliable PM emission measurement methods for marine engines has hindered the establishment of appropriate

regulations [7,18]. Therefore, efficient removal of PM emissions from marine diesel engines remains a major technological challenge. Novel technologies need to be investigated to reduce PM pollution effectively. A limit on PN (the number of particles with a diameter over 23 nm) was added to Regulation (EU)2016/1628. The gradual introduction of PN emission control is also one of the trends in ship emission precision control development in the future. As PM is harmful and emission regulations are becoming increasingly strict, conducting relevant research on controlling PM emissions from marine diesel engines has become imperative, with significant theoretical and practical importance.

According to the analysis of Sobczyk et al. [19] of current techniques for removing PM from diesel engines, electrohydrodynamic methods are a viable solution for effectively eliminating PM from marine diesel engines. Five common particulate removal methods and their removal efficiency and limitation are listed in Table 1. The method of electrified water spray can achieve remarkably high efficiency in capturing PM, even for very small particles. The vessel wet electrostatic scrubber (WES) is a technology that employs this method to reduce particle emissions from marine diesel engines. An experimental work by Di Natale et al. [20] proved that this method provides higher removal of SO₂ and particulate matter compared to a conventional wet scrubber. As shown in Figure 1, in this type of scrubber, the gas stream flows through a scrubber tower that contains a liquid film or droplets that are charged with high voltage electrodes. As the gas stream passes through the WES, the charged liquid droplets attract the charged particles in the gas stream due to electrostatic forces. The electrostatic force plays a crucial role in the particle capturing efficiency of the vessel wet electrostatic scrubber, as it increases the capture efficiency of the scrubber by attracting more particles to the charged liquid droplets. Researchers have made diligent efforts to apply this technology to boat exhaust emissions.

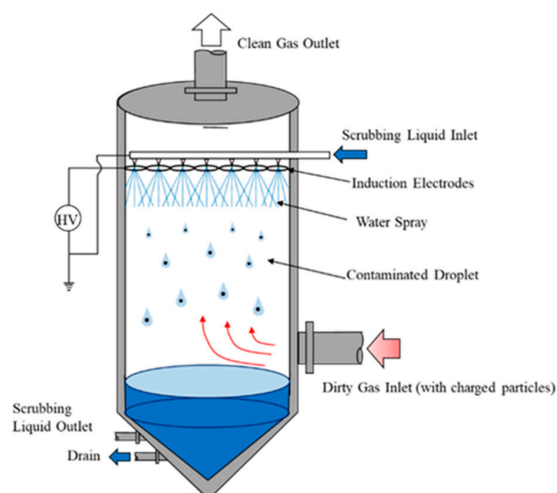


Figure 1. An example of vertical scrubber with a counter-current gas flow.

Table 1. Comparison of methods applied for marine vessel diesel PM emissions [19,21].

Method Applied in Marine Vessels	Reduction of PM Emission	Limitation
Fuel-borne additive	35%	Lowest reduction efficiency among those methods
Venturi scrubber	Over 90%	High pressure drops
Wet scrubber	<70% for submicron particle 70–99% for >PM1.0 About 50% for <PM1.0	Affected by many factors in scrubber
Electrostatic precipitator	80–93%	Re-entrainment of particles after a certain time operation
Electrified water spray	Capture efficiency over 95% (<PM0.4)	Operational characteristics are not yet fully understood

Numerical and experimental techniques are both employed to investigate the elimination of particles in wet electrostatic scrubbers [22–26]. Jaworek et al. [27,28] performed detailed theoretical and simulated work about both charged particles and droplets. In their theoretical work, they described the coordinate motion of a droplet–particle system using Newton’s vector differential equations, in which aerodynamic drag and image-charge effects were considered. Then, Krupa et al. [29] proposed a theoretical basis for the electrohydrodynamic of submicron particles, which can describe the droplet–particle intersection movement in a wet electrical scrubber, but without derivation and analysis. Through a wet electrostatic scrubber experiment examining high sulfur heavy fuel oil and marine gas oil, the researchers analyzed PM removal efficiency of charged or non-charged particles and different engine loads. The results showed that PM is efficiently removed from diesel engine exhaust by using a wet electrostatic scrubber system. D’addio et al. [30] conducted an experimental study in the context of marine diesel engine emission control. They highlighted the advantages of the wet electrostatic scrubber compared to other PM removal methods. Their results showed that particle abatement efficiency increases dramatically when spray and particles are both charged with opposite polarities. If either the spray or the particles are not charged, the abatement efficiency does not change significantly. Tests were carried out in various conditions, which were wet scrubber, charged droplet, and opposite polarities charged droplet and particles, respectively [31]. The influences of different L/G (water flow rate/gas flow rate) on the removal efficiency were also considered in this paper. Furthermore, Hirotsugu Fujita [23] investigated the diesel particulate matter (DPM) emission control of marine diesel engines and conducted experiments on an electrostatic water-spraying scrubber, using both fresh water and sea water. Based on the numerical and experimental results, it can be concluded that the efficiency of particle removal is significantly higher when both particles and droplets carry opposite charges. However, it may be difficult to generalize the results due to variations in the operating conditions and scrubber gas characteristics used in the experiments.

The basic mechanism of a WES involves capturing these small particles (even micron particles) by spraying charged droplets and applying electric forces to attract oppositely charged particles. Then, the droplets and settled particles are removed from the scrubber through a process of drainage or flushing. Diesel particles are mainly solid carbon (41%), unburned lubricant (25%), sulphate/water (14%), and other ash and unburned contents, which account for less than 20% of the DPM [32–34]. Zhou et al. [35,36] investigated the influence of fuel properties and particle size distributions on particle emissions from marine diesel engines. These researchers found that different types of diesel fuel oil have an effect on the specific emissions of total PM and its composition. Additionally, droplet size was found to be a critical parameter influencing the efficiency of particle capture. However, an exhaustive scientific description of charged particles being captured by charged droplets in a gas flow field is rare, as it typically lacks a clear understanding of the relationship between these parameters. Therefore, our goal is to clarify the mechanism underlying the movement of charged particles that are captured by charged droplets, and to develop a comprehensive scientific framework for the WES technology.

This paper presents an advanced mathematical model by coupling the particle movement model with the flow model around a spherical droplet under an electrostatic field. Additionally, a co-simulation model using ANSYS Fluent and MATLAB is established to validate the reliability of the mathematical model. To conduct the co-simulation research, computational fluid dynamics (CFD) software (ANSYS Fluent 2021) is used to establish a model of a charged particle moving in a gas flow field and being captured by a charged droplet. The effect of the electrical field on the particle movement process is then incorporated by calculations in MATLAB. The primary objective of this paper is to investigate the fundamental mechanism of capturing charged particles by charged droplets, particularly in the context of wet electrostatic scrubbers, with the aim of reducing the PM emissions from marine diesel engines and promoting the sustainable shipping practices.

2. Mathematical Model Mechanism

To reduce PM emissions from marine diesel engines that cannot be efficiently removed using conventional methods, a wet electrostatic scrubber appears to be highly effective. However, before implementing this technology on boats, a thorough understanding of the theoretical mechanism of particle and droplet transport is essential. Electro-hydrodynamics are utilized in the mechanical study of particle capture by charged droplets. For the theoretical model, there are some assumptions, as follows:

- Ideal steady incompressible viscous flow field;
- Laminar flow field;
- The black carbon particle and droplet are both single solid spherical particles;
- The droplet is static in the flow field, and the movement of the particle in the flow field around the liquid droplet is the main target considered in this study;
- The direction of gas flow and particle movement is vertical upward.

Analyzing the forces acting on charged particles captured by charged droplets is a necessary step to understand their movement characteristics. This preliminary analysis is crucial before establishing the equations that govern their motion. In this paper, an investigation is conducted under the setting of the particle moving in a vertical direction. As shown in Figure 2, the particle moves upwards with the gas in the vertical direction, and the direction of gravity is vertical and downwards.

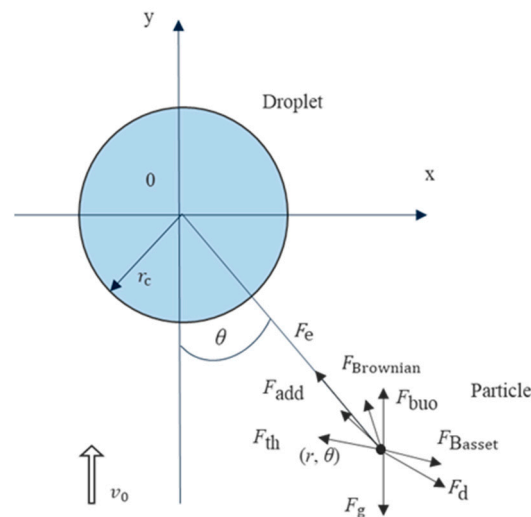


Figure 2. Forces acting on the particle and flow field near the droplet.

2.1. Particle Motion Equation

For a particle in fluid, gravity, added mass force, Basset force, thermophoresis, drag force, and Brownian force should all be taken into consideration, as shown in Figure 2. In addition to these common forces, because the particle and droplet are both electrified, electric force is the dominant force that exists in this research condition. Therefore, a vector differential equation can be used to describe the motion of a small-scale particle in an electric fluid field.

$$m_p \frac{du_p}{dt} = F_g + F_{buo} + F_{add} + F_d + F_{Basset} + F_{th} + F_{Brownian} + F_e \quad (1)$$

where m_p is the mass of a particle, u_p is the velocity of a particle, and F_g , F_{buo} , F_{add} , F_d , F_{Basset} , F_{th} , $F_{Brownian}$, and F_e are the gravity, buoyancy, added mass force, drag force, Basset force, thermophoresis force, Brownian force, and electrostatic force, respectively. Particles are suspended and move with the gas flow at the same velocity by default when there is no additional force. Thus, gravity and buoyancy can be ignored simultaneously.

The added mass force in Equation (1) is given by the following equation:

$$F_{add} = \frac{1}{2}\rho_f V_p \left(\frac{du_f}{dt} - \frac{du_p}{dt} \right) \quad (2)$$

where ρ_f is the density of gas fluid, V_p is the volume of particle, and u_f is the velocity of the flow field. In this study, the magnitude of the density ratio of gas and particle is approximately 10^{-3} , as shown in Table 2. Their velocity magnitudes are in the same order in this research. Thus, the impact of added mass force is not considered.

Table 2. Model properties.

Droplet radius/ r_c	0.1 mm, 0.5 mm, 1 mm, 2 mm
Particle radius/ r_p	5 μm , 10 μm , 20 μm , 50 μm
Density of particle/ ρ_p	$1.05 \times 10^3 \text{ kg/m}^3$
Density of gas fluid/ ρ_f	1.019 kg/m^3
Dynamic viscosity of gas fluid/ μ	$1.948 \times 10^{-5} \text{ Pa}\cdot\text{s}$
Inlet velocity of flow field/ u_0	5 m/s
Vacuum dielectric constant/ ϵ_0	$8.85 \times 10^{-12} \text{ F/m}$
Relative dielectric constant (particle)/ ϵ_{rp}	30
Relative dielectric constant (droplet)/ ϵ_{rc}	81.5

The drag force in the Equation (1) can be written in the following form:

$$F_d = 3\pi\mu d_p \left(1 + \frac{3}{16} Re \right) (u_f - u_p) \quad (3)$$

in which μ is fluid viscosity, d_p is the diameter of particle, and $Re = \frac{\rho_p d_p (u_f - u_p)}{\mu}$ is the Reynold number.

The Basset force can be described as follows:

$$F_{Basset} = \frac{3}{2} d_p^2 (\pi \rho_f \mu)^{1/2} \int_{t_0}^t (t - t')^{1/2} \left(\frac{du_f}{dt} - \frac{du_p}{dt} \right) dt' \quad (4)$$

in which t is the time period of the particle moving. The Basset force exists when particle moves in an unstable flow field, which is not the condition in this model assumption. Thus, this force is not considered in this study.

The thermophoresis force can be written as follows [37]:

$$F_{th} = 1.15 \frac{K_n}{4\sqrt{2}\alpha(1 + \frac{\pi_1}{2} K_n)} \left[1 - \exp\left(-\frac{\alpha}{K_n}\right) \right] \left(\frac{4}{3\pi} \phi \pi_1 K_n \right)^{1/2} \cdot \frac{k}{d_p^2} \nabla T d^2 \quad (5)$$

where $K_n = 2\lambda/d$ is the Kundsens number and k is the Boltzman constant. Equation (6) is as follows:

$$\phi = 0.25(9\gamma - 5) \frac{C_v}{R} \quad (6)$$

where $R = 287 \text{ J/kgK}$ and R is the fluid constant. $C_v = 718 + 0.1167\rho_f \text{ J/kgK}$, where C_v is the constant volume specific heat. $\gamma = 1.4$, where γ is the specific heat ratio.

$$\alpha = 0.22 \left[\frac{\frac{\pi}{6}\phi}{1 + \frac{\pi_1}{2} K_n} \right]^{1/2} \quad (7)$$

and

$$\pi_1 = 0.18 \frac{\frac{36}{\pi}}{(2 - S_n + S_t) \frac{4}{\pi} + S_n} \quad (8)$$

where S_n and S_t are the normal and tangential movement accommodation coefficients. For this study, the parameters were selected at a fixed temperature of 80°C . The change in the

temperature and the temperature difference between the gas and the liquid is not taken into consideration. Therefore, the effect of thermophoresis force resulting from temperature variations was not taken into consideration in this research.

The Brownian force effect is quite negligible when compared with the electrical force and drag force effect.

The electrostatic force can be given out in the following form proposed by A. Jaworek [38]:

$$F_e = \frac{Q_p Q_c}{4\pi\epsilon_0 r^2} + \frac{r_p Q_c^2}{4\pi\epsilon_0 r^3} \left(\frac{r^4}{(r^2 - r_p^2)^2} - 1 \right) + \frac{r_c Q_p^2}{4\pi\epsilon_0 r^3} \left(1 - \frac{r^4}{(r^2 - r_c^2)^2} \right) \quad (9)$$

where Q_p and Q_c are the charges on the aerosol particle and droplet, respectively, r is the distance between the particle and the droplet centre, and ϵ_0 is the permittivity of the free space. The first term on the left in the equation represents the Coulomb force and the other two terms represent the image force. The main electrostatic force considered here is the Coulomb force, since it has much more of an effect than the particle image force when the particle and droplet have opposite charges [39].

This study considers the drag force, F_d , and the electrostatic force, F_e , specifically the Coulomb force, as the predominant forces acting on the particle based on the theoretical model proposed in this paper.

2.2. Air Flow Field Distribution

According to the analysis of forces on the particle motion, as shown in Figure 2, particle motion characteristics are affected by the surrounding gas flow field distribution. This motion mechanism coupled the particle velocity, gas flow field velocity, particle position, and also the electrostatic field strength in our research. Thus, a coupled mathematical model is needed to describe the particle–droplet intersection motion characteristics under the condition of an electrostatic field. In this study, the stream function φ is utilized to obtain the velocity distribution around a sphere droplet. The equations are as follows:

$$\begin{cases} \nabla^2 \varphi = 0 \text{ (in flow field)} \\ \frac{\partial \varphi}{\partial r} = 0 \text{ (on the surface of droplet)} \end{cases} \quad (10)$$

$$\frac{\partial \varphi}{\partial r} = u_0 \cos \theta; \frac{\partial \varphi}{r \partial \theta} = -u_0 \sin \theta \text{ (at infinity)}$$

After derivation, the velocity distribution can be described as follows:

$$u_r = \frac{\partial \varphi}{\partial r} = u_0 \cos \theta \left(1 - \frac{r_c^2}{r^2} \right) \quad (11)$$

$$u_\theta = \frac{1}{r} \frac{\partial \varphi}{\partial \theta} = -u_0 \sin \theta \left(1 + \frac{r_c^2}{r^2} \right) \quad (12)$$

Functions (11) and (12) describe the gas flow velocity distribution around a sphere, where u_r represents radial velocity component and u_θ represents the angular velocity component. For the research work of this article, the value of θ is set to 0. The velocity of the gas flow field surrounding a particle can be determined based on the distance between the particle and droplet. Using simultaneous equations of the air velocity distribution around the droplet and the particle motion equation, a mathematical model can be obtained to describe the motion of a charged particle around an oppositely charged droplet in a gas flow field. The mathematical model is presented in Equations (13)–(15). By determining the motion characteristics of particles in the flow field around the droplet, the mechanism behind the capture of small-scale particles by electrostatic liquid droplets can be explained in detail.

$$m_p \frac{du_p}{dt} = -3\pi\mu d_p \left(1 + \frac{3}{16} Re \right) (u_f - u_p) + \frac{Q_p Q_c}{4\pi\epsilon_0 r^2} \quad (13)$$

$$u_f = u_0 \cos\theta \left(1 - \frac{r_c^2}{r^2}\right) \text{ (Gas flow field around sphere droplet)}. \quad (14)$$

The relationship of a particle or a droplet saturation charge Q with E and d is as follows:

$$Q = \frac{3\varepsilon_r}{\varepsilon_r + 2} \pi \varepsilon_0 d^2 E \quad (15)$$

where d is diameter, ε_r is the relative dielectric constant, ε_0 is the dielectric constant of vacuum whose value is 8.85×10^{-12} F/m, and E is the electric field strength.

The ultimate charge of a liquid droplet is known as Rayleigh limit, and it is calculated as follows [40]:

$$Q_{dc} = 8\pi \left(\varepsilon_0 \sigma_c r_c^3\right)^{1/2} \quad (16)$$

where σ_c is surface tension of droplet, the value of which is 71.95×10^{-3} N. For the condition shown in Table 2, the value of Q_{dc} is 6.342×10^{-10} . When the electrostatic field strength is 10 kV, the droplet charge Q is 3.256×10^{-12} , which is much less than the limit value.

3. Mathematical Results and Discussion

To verify the effect of the electrostatic field on the particle capture process, different parameters are introduced into Equation (14). By solving the equation under these series of conditions, particle motion characteristics under different variable factors can be obtained. Here, the effect on the charged particle motion of electric field strength, particle size, and droplet size are mainly considered. The equations are solved using the fourth-order Runge–Kutta method. Parameters chosen when solving the equations are listed in Table 2. The angle of particle moving towards the droplet, θ , is set to 0 to simplify the equation solving.

Firstly, particle motion characteristics are compared in the presence or absence of electrical forces. In the process of the theoretical calculation, the particle was defined as moving towards the vertical axis of the droplet. In this research, collision and rebound were not considered. The droplet radius was 1 mm. When the distance between a particle and the center of a droplet is less than 1 mm, it is considered that the particle has been captured by the droplet theoretically. The initial distance between a particle and the center of a droplet is set to 6 mm here, which means that the distance between the particle and the surface of the droplet is 5 mm. The distance in the figures represents the distance between the particle and the droplet surface. When $t = 0$ ms, the distance represents the initial distance of the particle in flow field around the droplet. When the distance is equal to 0 mm, this represents when the particle reaches the droplet surface. The initial particle velocity equals the flow velocity of the particle initial position in the flow field. The trends of distance, with and without an electric field, are shown in Figure 3. The Y-axis represents the distance from the particle to the droplet surface. It can be seen from the figures that the changing trend of the two curves is generally similar whether the electric field exists or not. That means the times of particles reaching the droplet were almost the same under these two conditions, taking approximately 1.05 ms, as shown in Figure 3.

As for the trend of the particle velocity, it can be illustrated from Figure 4 that the electrostatic force can help increase the velocity of the particle when it moves close to the droplet. The velocity difference was 0.028 m/s before the particle was captured by the droplet.

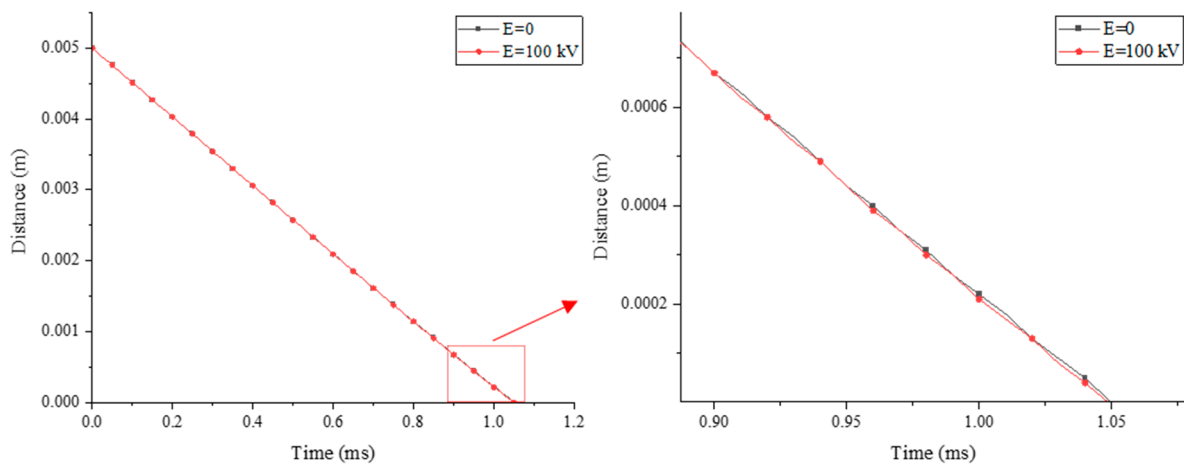


Figure 3. Trends of distance change with and without electric force when the droplet radius is 1 mm and the particle radius is 10 μm .

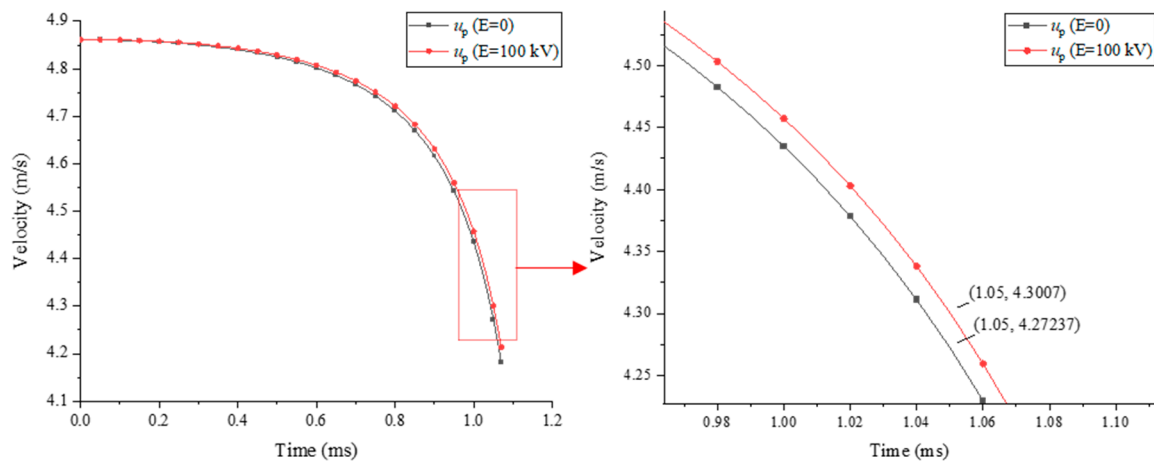


Figure 4. Trends of velocity change with and without electric force when the droplet radius is 1 mm and the particle radius is 10 μm .

To verify the influence trend and the extent of each factor, different electric field strengths, droplet radii, and particle radii are defined when solving the equations. Thus, a series of trend changes in the distance and velocity can be concluded.

When comparing different electric field strengths (0 kV, 30 kV, 50 kV, 100 kV), it can be concluded from Figure 5 that the greater the electric field strength, the greater the velocity before the particle is captured by the droplet. However, this effect is not significant.

The magnitudes of drag force F_d and electric force F_e are compared in Figure 6, when the electric field strength was 100 kV. The forces are presented using a logarithmic scale to show their magnitudes more clearly. It can be seen that the magnitude of the electric force was far less than that of the drag force even though the electric field strength was 100 kV. Therefore, simply improving the electrostatic field strength will not obviously influence the process of particle motion.

Figures 7 and 8 depict the movement tendency of particles of different sizes (5 μm , 10 μm , 20 μm , and 50 μm) under identical electric field strength (20 kV). The tendency indicates that larger particles are easier to capture with the droplet. In Figure 7, the 50 μm particle reaches the droplet's radius more rapidly than other particles. The capture time of the 50 μm particle is approximately 1.028 ms, while the capture time of the 20 μm particle is 1.035 ms, the capture time of the 10 μm particle is 1.051 ms, and the capture time of the 5 μm particle is 1.103 ms.

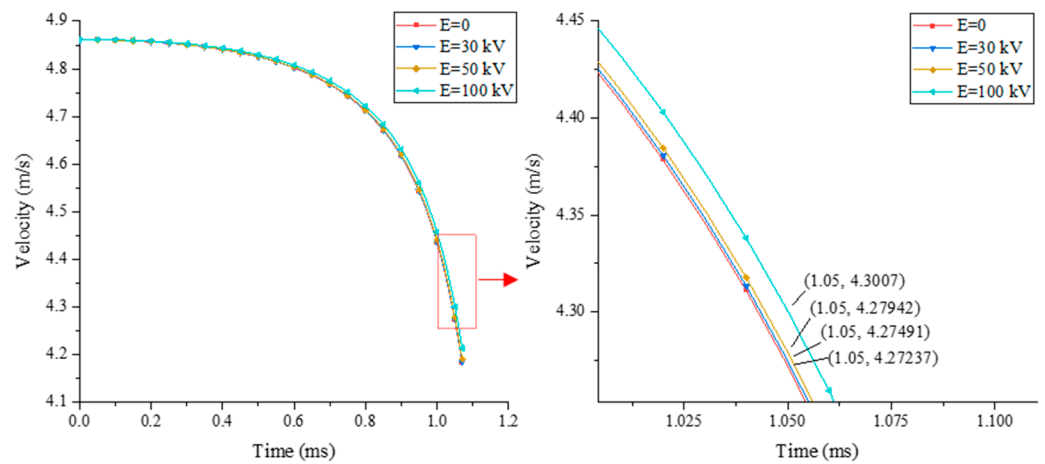


Figure 5. Trends of velocity change under different electric field strengths when the droplet radius is 1 mm and the particle radius is 10 μm .

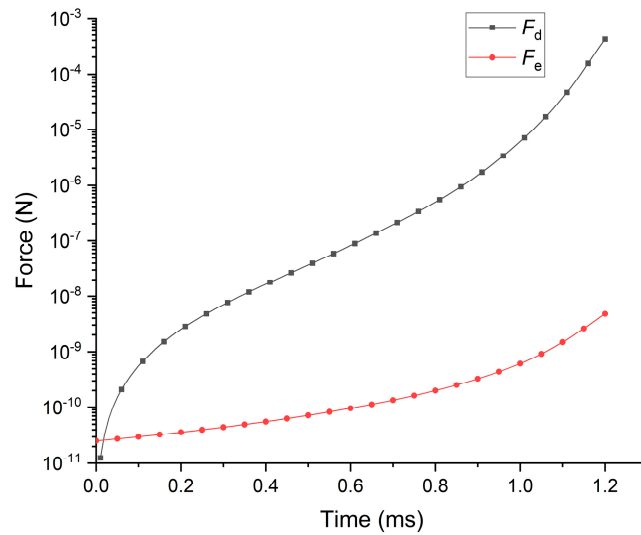


Figure 6. Magnitude comparison of drag force and electric force when the droplet radius is 1 mm and the particle radius is 10 μm .

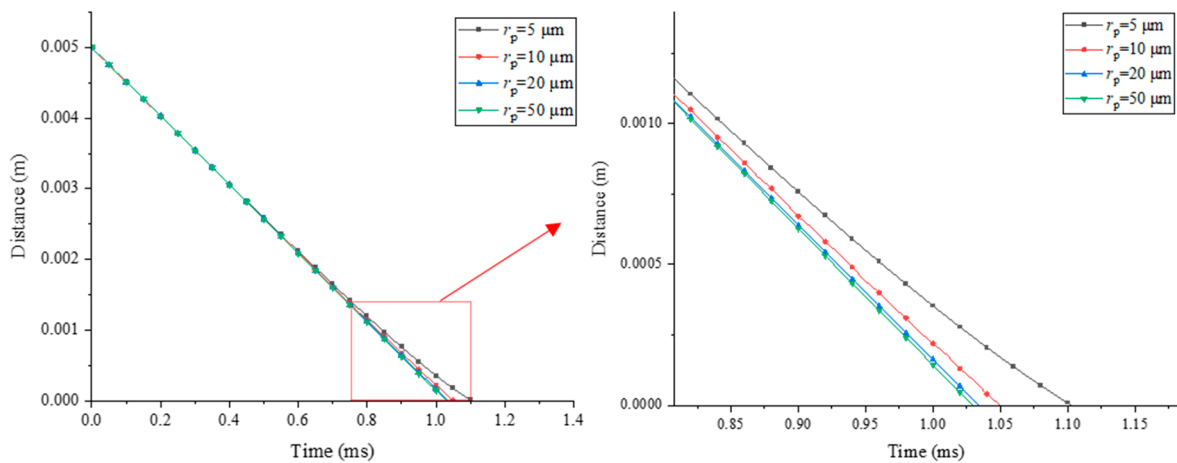


Figure 7. Trends of distance change under different particle diameters when droplet radius is 1 mm and electric field strength is 20 kV.

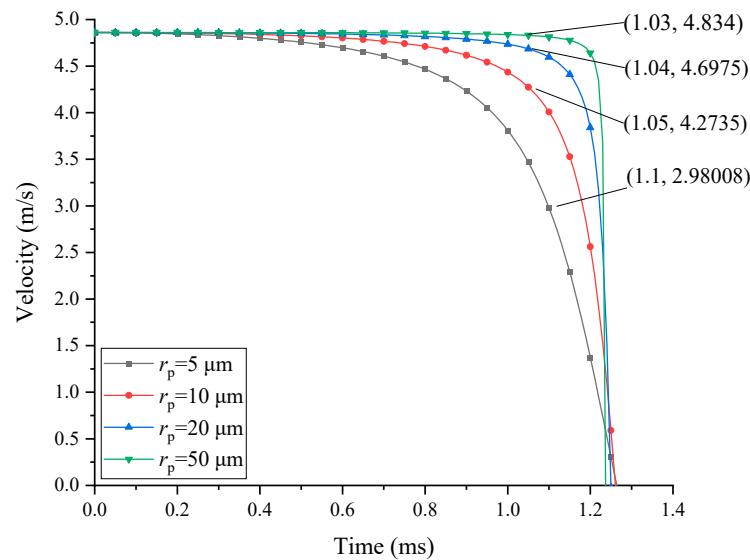


Figure 8. Trends of velocity change under different particle diameters when the droplet radius is 1 mm and the electric field strength is 20 kV.

In Figure 8, the velocity of particles decreases with time as the particles move closer to the droplet. Before the particles were captured, the particle velocity of 50 μm is much greater than that of 5 μm . According to the results of Figure 7, the time when particle reaches the droplet surface can be obtained. It is annotated in Figure 8, and the difference in particles velocities of different sizes is obvious. For the particle size below 10 μm , when the particle radius decreases by 50%, from 10 μm to 5 μm , the particle velocity of reaching the droplet surface decreases by 30.28%. For particle sizes beyond 10 μm , the velocity is still over 4 m/s before arriving the droplet surface. When particle radius decreases from 20 μm to 10 μm , the change in radius is large, but the particle velocity reaching the droplet surface only decreases by 9.01%. This indicates that under the electrostatic field condition, for particle size beyond 10 μm , the influence of particle size is not sharp. Thus, the electrostatic effect was much greater for larger particles.

Figures 9 and 10 present the results of particles' movement with different droplet sizes (0.1 mm, 0.5 mm, 1 mm, and 2 mm) under identical electric field strength (20 kV). The times when these particles arrived at the droplet surface were 1.021 ms, 1.031 ms, 1.051 ms, and 1.097 ms, respectively. Comparing the results in Figure 9, the distance between the particle and the droplet decreases over time for all droplet diameters. The curves are initially linear, indicating a constant velocity, but then they start to curve as the distance decreases, indicating a reduction in velocity. As shown in Figure 9, when the distance is 0 m, that means the particle reaches the droplet surface. For larger droplets ($r_c = 2$ mm and $r_c = 1$ mm), the distance decreases more gradually compared to smaller droplets ($r_c = 0.5$ mm and $r_c = 0.1$ mm). This implies that particles approaching larger droplets slow down earlier and more gradually than those approaching smaller droplets. It can be concluded that smaller droplets can attract the particle more quickly.

Figure 10 shows that the size of droplets has a significant impact on particle velocity. When the droplet size is small (the radius is 0.1 mm), the particle keeps moving at a relatively high speed before arriving at the droplet surface. As shown in Figure 10, at the moment that it is attracted by the droplet, the particle's velocity is 4.86 m/s, 4.58 m/s, 4.27 m/s, and 3.75 m/s, respectively, when the droplet radii are 0.1 mm, 0.5 mm, 1 mm, and 2 mm. This implies that when droplet size decreases by 50% from 2 mm to 1 mm, the final particle velocity increases by 13.85%. When droplet size decreases by 50% from 1 mm to 0.5 mm, the final particle velocity increases by 7.26%. The increase in final particle velocity is significant with the decrease in droplet size. Figure 11 illustrates the ratio of drag force to electrostatic force acting on a particle in the present research work. This figure

helps explain the results analyzed regarding the relationship between the F_D/F_E and r_c/r_p . The four cases presented correspond to the same position ($r = 0.0001$ mm) near the droplet surface. The results suggest that droplets size has an influence on the velocity distribution of the gas flow field around the droplet. Simultaneously reducing the droplet size can lead to a diminished impact of the drag force. While this reduction also lessens the influence of the electrostatic force, it is important to note that the drag force plays a more dominant role in the particle motion process. Consequently, a decrease in droplet size can effectively facilitate the accelerated capture of particles.

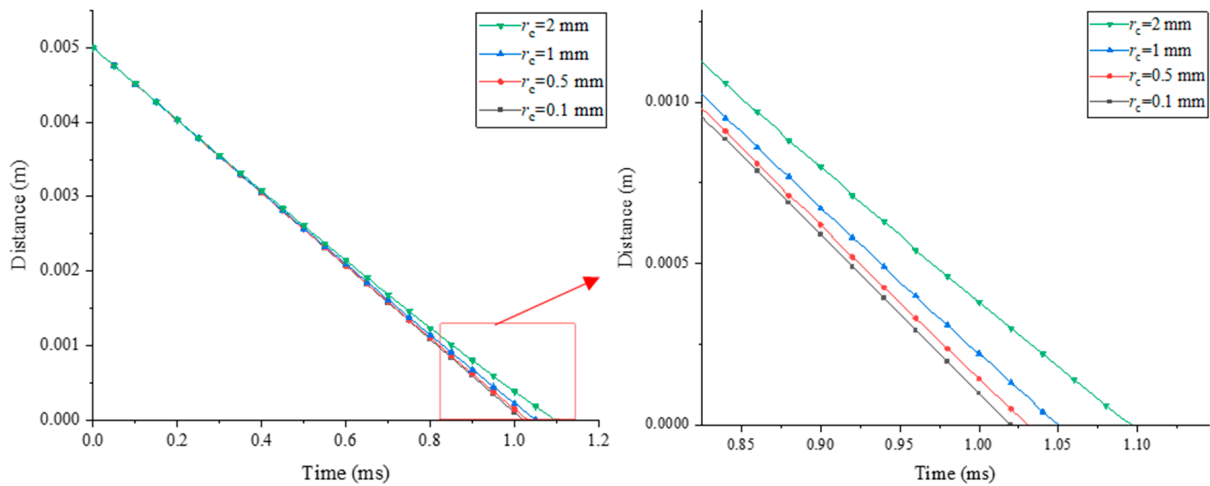


Figure 9. Trends of distance change under different droplet diameters when the particle radius is 10 μ m and the electric field strength is 20 kV.

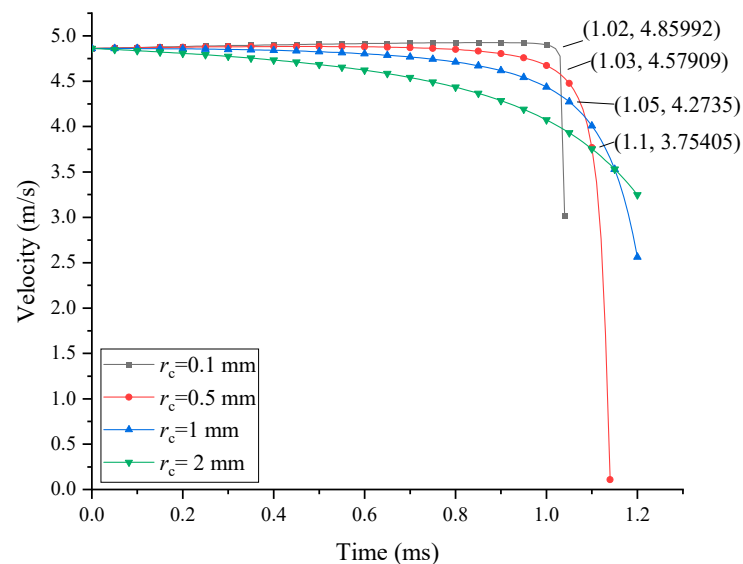


Figure 10. Trends of velocity change under different droplet diameters when particle radius is 10 μ m and electric field strength is 20 kV.

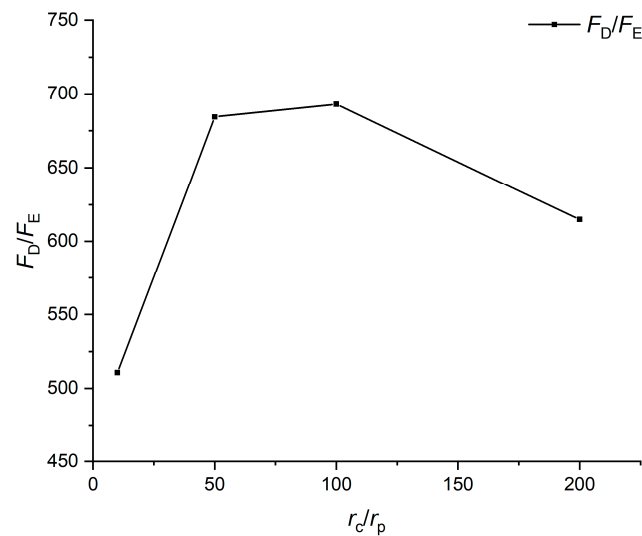


Figure 11. Drag force to electrostatic force ratio (F_D/F_E) as a function of droplet to particle size ratio (r_c/r_p).

4. Co-Simulation with ANSYS Fluent and MATLAB

4.1. Co-Simulation Mechanisms

For the simulation of particle motion, in this study, a co-simulation approach using ANSYS Fluent 2021 and MATLAB 2022 was employed to realize a coupled simulation of the flow field and electrostatic field. The flow field distribution around the particle and the droplet obtained from the ANSYS Fluent 2021 simulation is combined with particle movement models that take the presence of electrostatic fields into account. The flowchart of the computational procedures for the co-simulation approach is shown in Figure 12. As shown in this figure, running the command code in MATLAB 2022 results in the initialization of Fluent, and the reading of data from the monitoring points. The monitoring points are points chosen around the particle and move with the overset system. Overset meshing involves creating multiple overlapping meshes that cover different parts of the computational domain. These meshes are allowed to overlap with each other, and the solution is interpolated between the meshes in the overlapping regions. This approach is particularly useful for modelling moving parts within a fixed background mesh without the need for remeshing and allowing localized mesh refinement by using finer meshes in regions of interest without affecting the global mesh. In the computational procedures, the velocity of the monitoring point, which represents the flow field velocity at the particle's position, was read into MATLAB 2022 for the calculation of particle movement in MATLAB 2022. During the solving of the particle movement equation, in addition to the basic movement laws of sphere particles in a flow field, the function of the electrostatic force was added to the computational process. Then, a description of particle motion at this moment in a gas flow field under the action of a charged droplet in an electrostatic field was obtained. A user-defined function (UDF) was employed to incorporate the effects of electrostatic fields into the simulation procedure. However, the MATLAB 2022 solution needed to be converted into the C language, which could be recognized by Fluent, before being written into the UDF file. Then, the motion UDF was compiled in the Fluent 2021 software to complete the particle motion simulation. The next step was judging whether the particle was captured by the droplet after simulating it under a given time step size. If not, the updated flow field data of the monitoring points were rewritten into MATLAB to complete the next iteration. Iterative computation was finished when the particle arrived at the droplet surface. Thus, the simulation of the particle moving towards the droplet under the influence of an electrostatic field was obtained.

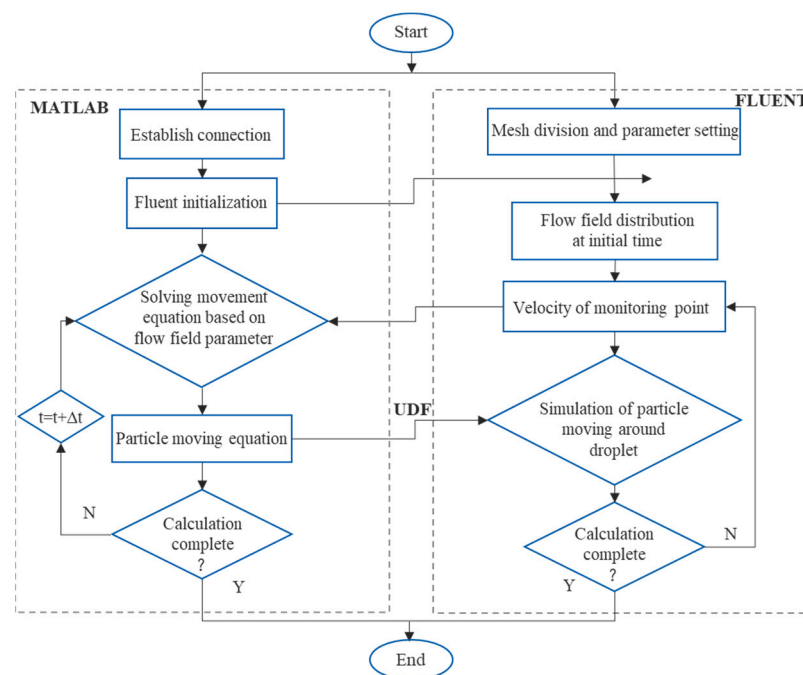


Figure 12. Flow chart of the computational procedures for the co-simulation approach.

4.2. 3-D Numerical Model

The particle motion numerical model in a wet electrostatic scrubber is shown in Figure 13. The model consists of a cylindrical flue gas channel ($100 \text{ mm} \times \text{Ø}50 \text{ mm}$), a flue gas inlet, and an outlet at both ends of the round-through. Detailed design parameters of the model are presented as the properties in Table 2. The gravity direction is the opposite direction of the X -axis. During the simulation, it was found that the effect of electrostatic force is not obvious when the particle was far from the droplet. Thus, the initial distance between the droplet and particle was defined as 6 mm in this simulation model. Figure 13 shows the general configurations of the boundary conditions. The inlet velocity was set at the upstream inlet boundary, below the surface of the tube. Here the fluid material that fully filled the tube was air, whose parameters are the same as flue gas, as shown in Table 2. The droplet material is defined as solid without considering its movement and deformation.

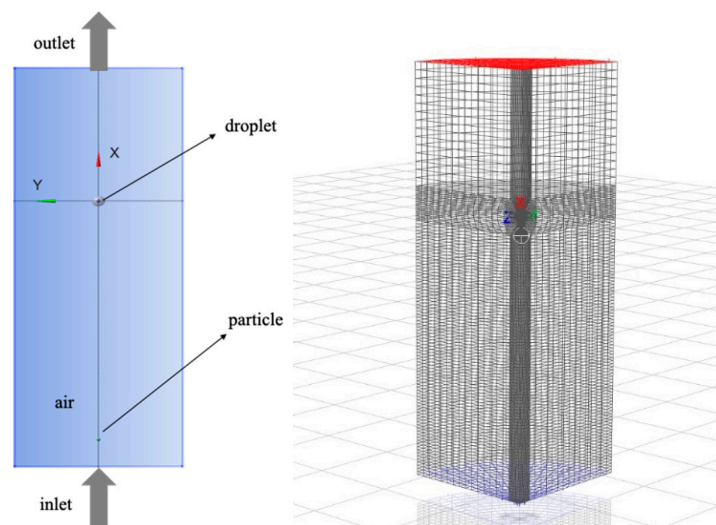


Figure 13. Coupled motion model of the particle and droplet for simulation.

Since the model is a rotationally symmetrical structure, to improve the calculation accuracy and operation efficiency, only a quarter of the model is considered in the simulation. According to the mainstream and flow field distribution, the model mesh was divided into several parts and locally refined as well, as shown in Figure 13. The particle motion simulation is based on an advanced overset moving grid method that accurately considers the local and global motion of a three-dimensional wet electrostatic scrubber. The overset mesh system consists of the background mesh, which is the whole computational fluid domain, and the refined overlapping meshes. In the present study, as shown in Figure 14, a sphere overset mesh was designed outside the particle to compute the flow field distribution around the moving particle.

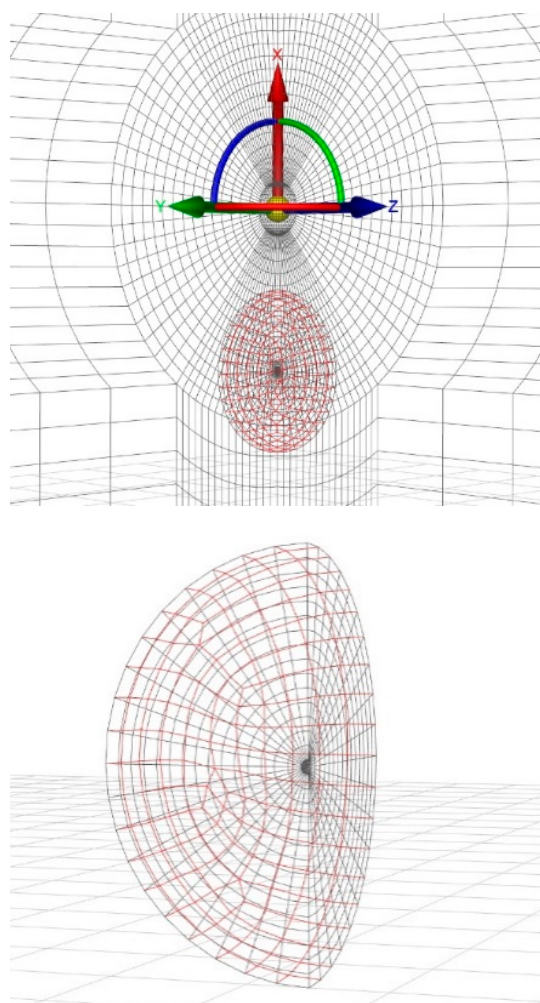


Figure 14. Illustration of the particle overset mesh.

4.3. Co-Simulation Results and Discussion

In the co-simulation of flow field distribution in the cylindrical flue gas channel around a solid sphere, the model used is the standard k-epsilon viscous model. The kinetic energy and turbulent dissipation rate equations are both first-order upwind. The particle movement is simulated by adding the motion function on the overset mesh. The motion function, which takes the electrostatic force into consideration, is solved in MATLAB and then written into a UDF file. Figure 15 shows a contour plot of the velocity magnitude when the particle is approaching the droplet. It can be seen in this figure that under the presence of electrostatic effect, the velocity of the particle is much greater than that of the surrounding flow field when the particle approaches the droplet surface. Through

changing certain model parameters and electrostatic field strengths, the simulation results of particle motion characteristics under some features were investigated.

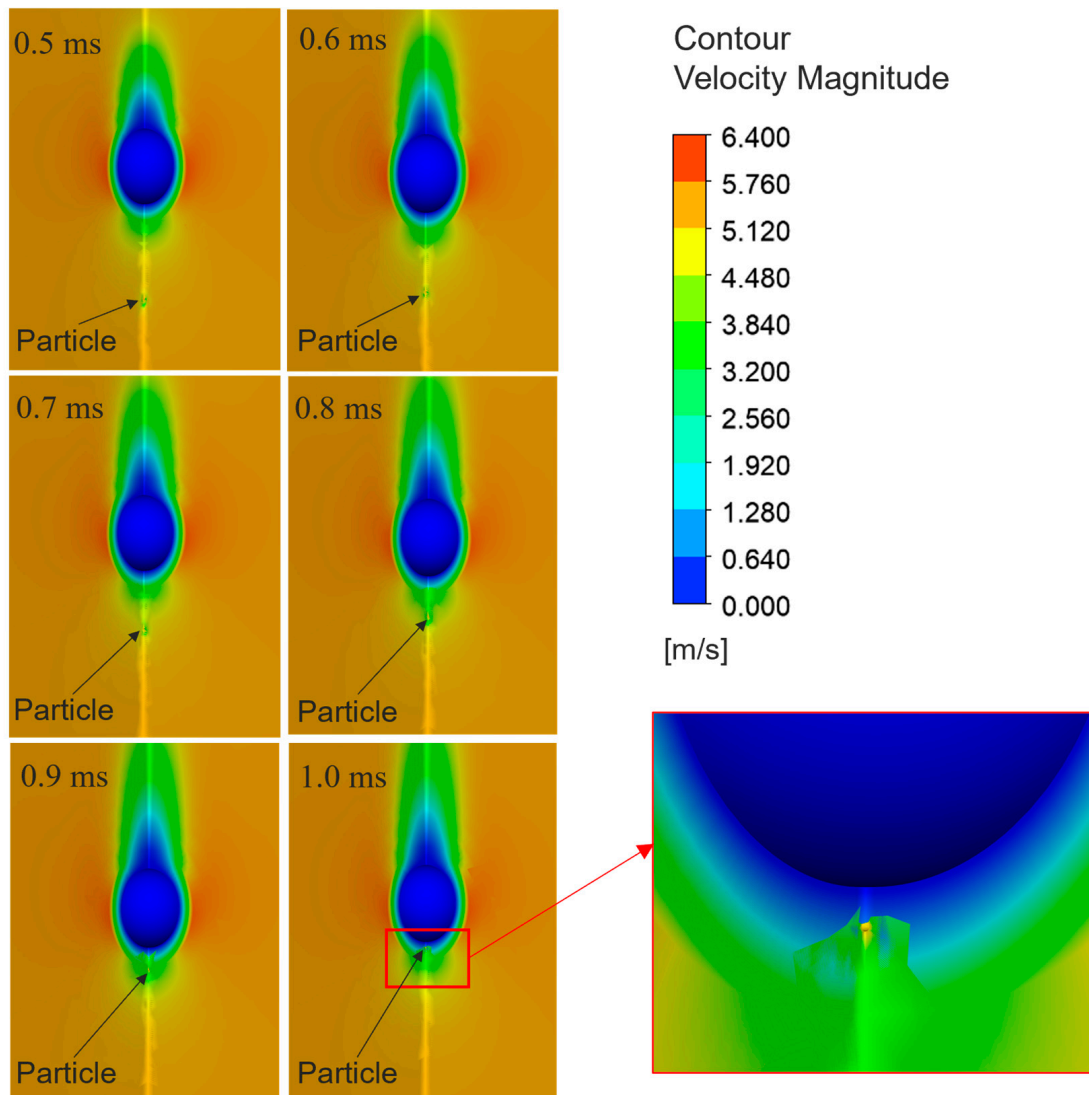


Figure 15. Contour plot of the velocity magnitude when the particle is approaching the droplet when the droplet radius is 1 mm, the particle radius is 10 μm , and the electric field strength is 20 kV.

Through the method of co-simulation of ANSYS Fluent 2021 and MATLAB 2022, the entire process of a charged particle moving towards the charged droplet in a fuel gas flow field under the effect of electrostatic force can be described. In the meanwhile, the influence of some features on the movement characteristic can be observed by changing the corresponding parameters during the simulation. In Figure 16, the changing tendencies of particle velocity solved in the simulation and mathematical model are compared under the electrostatic field strength of 20 kV. The changing trends in these two results show general consistency. The difference between these two results in the last part of Figure 16 is mainly because the influence of the droplet surface on the flow field is ignored in the mathematical calculation, while the droplet surface is regarded as the wall surface in simulation. As a result, the velocity is zero when the particle reaches the droplet surface in the simulation, which is not the case in the mathematical calculation. As a whole, to describe the particle motion characteristics under electrostatic field before it arrives at the droplet surface, the simulation and theoretical results are basically consistent.

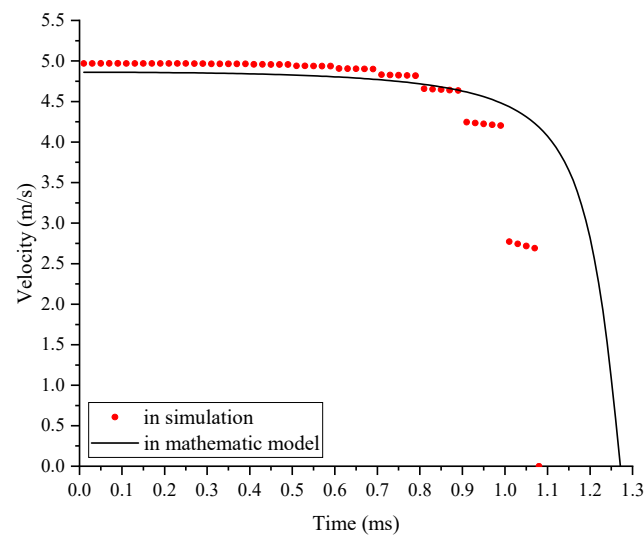


Figure 16. Comparison of simulation and theoretical results under the electric field strength of 20 kV.

Referring to the theoretical results, motion processes of different particle sizes and droplet sizes under electrostatic field strength of 20 kV were simulated in this section. Figure 17 demonstrates the velocity change trend with the time of different particle radii (10 μm , 20 μm , 50 μm). Compared with the mathematical result in Figure 8, a consistent conclusion is obtained in Figure 17 that the larger the particle, the greater its velocity will be before being captured. Meanwhile, the velocity of the particle is zero when it arrives at the droplet surface in the simulation. Thus, the time when the velocity equals zero means that the particle arrives at the droplet surface. In Figure 17, under the same movement conditions, for particles with radii of 10 μm , 20 μm , and 50 μm , the lengths of time for them to reach the surface are 1.079 ms, 1.031 ms, and 1.010 ms, respectively. The results show that the larger particles are captured faster than the smaller ones under the effect of electrostatic force.

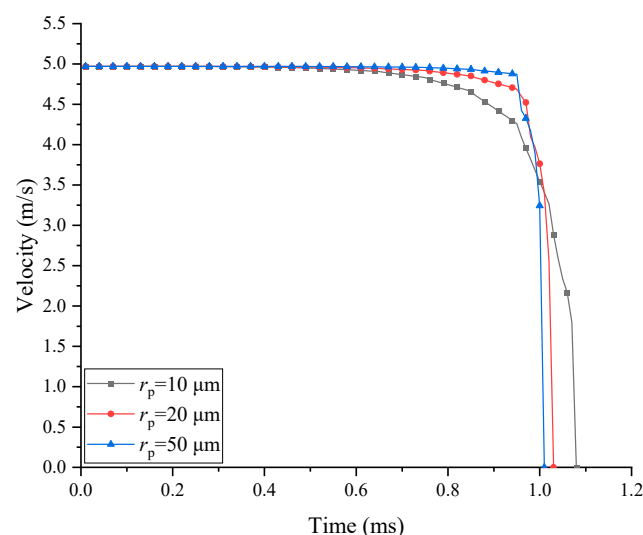


Figure 17. Comparison of the velocities of particles with different particle radii when the droplet radius is 1 mm.

As for different droplet sizes, the co-simulation results of velocity change trends are shown in Figure 18. The velocity change tendency of three droplet sizes (0.5 mm, 1 mm, 2 mm) are basically the same as in Figure 10. The tendency indicates that the smaller droplet shows a better capture effect. For droplet radii of 0.5 mm, 1 mm, and 2 mm, the time for particles to reach the droplet surface is 1.018 ms, 1.052 ms, and 1.121 ms, respectively.

Meanwhile, the flow field distribution around the droplet is affected by the droplet size. The increase in droplet size decreases the effect of drag force and increases the effect of electrostatic force. Thus, the velocity of the particle around smaller droplets is greater than that around larger droplets.

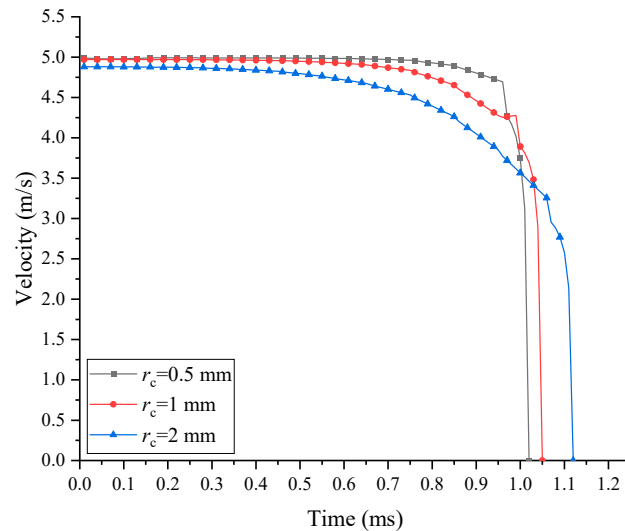


Figure 18. Comparison of the velocities of particles with different droplet radius values when the particle radius is $10\ \mu\text{m}$.

Comparing the particle velocity change trend in the mathematical and simulation results in Figure 16, it is found that the velocity change curve in the theoretical results is slightly lower than that of the simulation curve. This is because the surrounding gas flow field velocity is affected by the moving particle, which is ignored in the theoretical calculation. Figure 19 shows the velocity distribution around the droplet and moving particle. It can be seen in this figure that the flow field around the particles is affected by moving particles. The velocity of the particles on the windward side increases and the velocity on the leeward side decreases. However, in this simulation condition, the affected area is not large when compared with the droplet size. Then, the velocity distributions of particle and flow field during particle motion are conducted when particle sizes are $10\ \mu\text{m}$ and $20\ \mu\text{m}$.

The change in the velocity distribution of the flow field along the particle motion path during the motion process is obtained in the simulation. Figure 20 shows the velocity distributions of 0.2 ms, 0.4 ms, 0.6 ms, and 0.8 ms of particle size $10\ \mu\text{m}$ and $20\ \mu\text{m}$, respectively. The horizontal coordinate represents the position on the motion path. Zero on the horizontal coordinate is the spherical center of the liquid droplet, whose radius is $1\ \text{mm}$. As can be seen in this figure, during the process of particle motion, the velocity difference between the particle and the gas flow field increases as the particle approaches the droplet. Comparing the velocity distribution of gas flow field of size $10\ \mu\text{m}$ and size $20\ \mu\text{m}$ particles, it is found that the larger particle has a greater impact on the flow field around it. This impact is mainly manifested in the reduction in flow field velocity in the area where the particles pass through.

The mathematical calculation and simulation results under the condition of 20 kV electrostatic field strength are summarized in Table 3. Comparing the particle movement characteristics under different particle sizes and droplet sizes, the conclusions obtained from the previous analysis in this paper are more apparent in this table. Furthermore, the results for the time it takes for particles to reach the droplet surface in this table are compared in the mathematical calculation and in the simulation under the same conditions. The relative error ranges from 0.4% to 2.6%, and the average error is 1.5%.

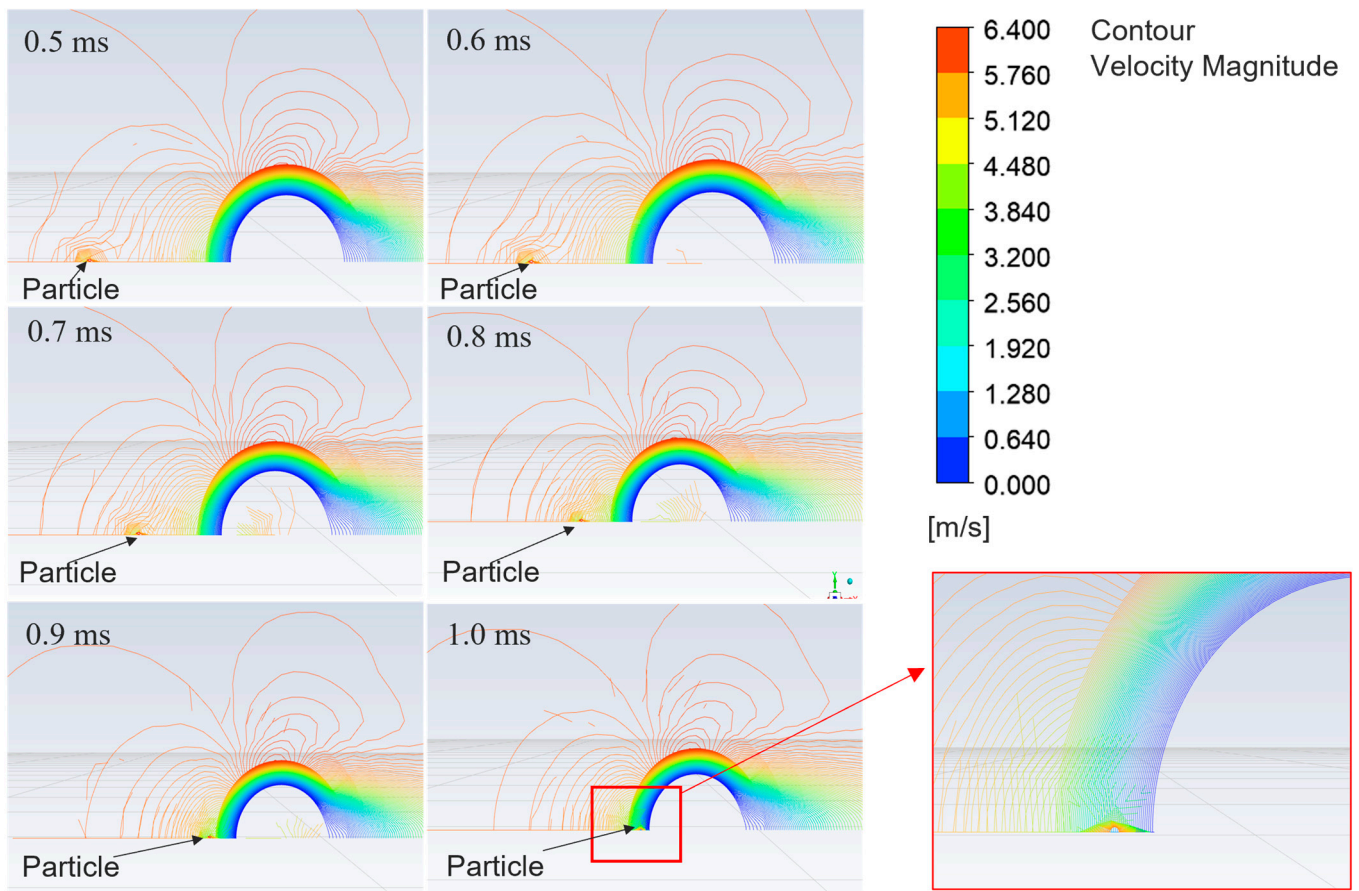


Figure 19. Side view of instantaneous velocity magnitude profiles when the droplet radius is 1 mm, the particle radius is 10 μm , and the electric field strength is 20 kV.

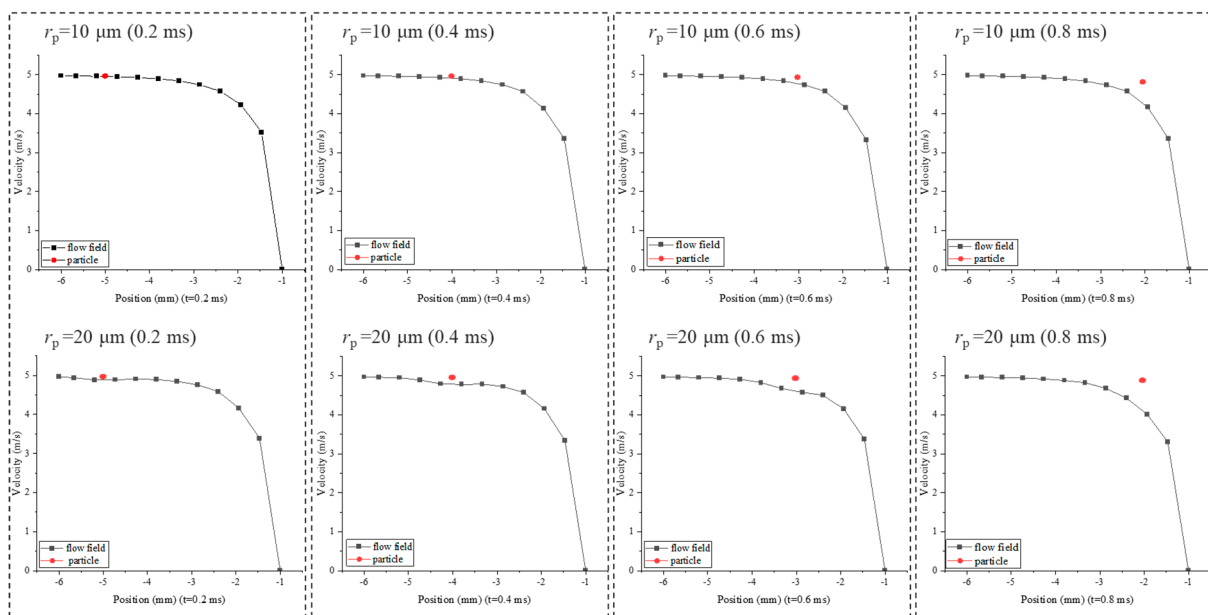


Figure 20. Instantaneous velocity distribution plots of particle and flow field when the droplet radius is 1 mm and the electric field strength is 20 kV.

Table 3. Results of mathematical calculation and simulation.

	r_p (μm)	t (ms)	$\Delta\epsilon$	r_c (mm)	t (ms)	$\Delta\epsilon$
In theory	10	1.051	2.6%	0.5	1.031	1.3%
In simulation		1.079			1.018	
In theory	20	1.035	0.4%	1	1.051	0.9%
In simulation		1.031			1.052	
In theory	50	1.028	1.8%	2	1.097	2.1%
In simulation		1.010			1.121	

t : time length for the particle to arrive at the droplet surface, $\Delta\epsilon$: relative error.

The mathematical calculation results and co-simulation results are basically consistent, which indicates that the two methods are both reliable for describing the process of a charged particle moving in gas flow field when attracted by charged droplet. The existence of an electrostatic field can improve the particle velocity when it approaches the droplet, making the velocity greater than that of the surrounding flow field. Meanwhile, this effect is much more obvious with the particle approaching the droplet. Furthermore, the simulation results show that the moving particle can affect the surrounding velocity of the gas flow field, which is ignored in the theoretical calculation. This effect becomes more apparent as the particle size increases.

5. Conclusions

The mechanism of the particle motion towards a droplet under the effect of electrostatic field is studied in this work. In this condition, particles suspended in gas are attracted by a droplet under the effect of both the gas flow field and the electrostatic field. In this paper's research, based on the theoretical model assumption and solution, a mathematical model is obtained to describe the particle droplet motion characteristic under the condition of an electrostatic field. Analysis of the mathematical description indicates that electrostatic field strength, particle size, and droplet size are the key parameters which affect the motion characteristics. Then, through co-simulation with ANSYS Fluent and MATLAB, the simulation of the particle motion being captured by the droplet was performed, which verified the reliability of the mathematical model. Based on the analysis made in this study, conclusions can be drawn as follows:

- (a) The existence of an electrostatic field can improve the particle velocity when it approaches the droplet, making the velocity greater than that of the surrounding flow field. Meanwhile, this effect is much more obvious with the particle approaching the droplet.
- (b) Analysis of the effect of electrostatic field strength found that electrostatic force helps increase the particle capturing efficiency by attracting particles to the droplet but that it is not possible to increase the particle velocity significantly by increasing the electrostatic field strength, since the magnitude of the electrical force was far less than that of the drag force. Thus, a proper electrostatic field strength range is supposed to be defined in a follow-up research work.
- (c) The investigation of particle size shows that the electrostatic effect is much greater for larger particles. The effect of particle size is different for the range of particle radii. Under the electrostatic field condition (20 kV), for particle sizes beyond 10 μm , when the particle radius decreases by 50%, the particle velocity when reaching the droplet surface decreases by 9.01%. While the particle radius is below 10 μm , the particle velocity when reaching the droplet surface decreases by 30.28% when the particle size decreases by 50%.
- (d) Furthermore, the droplet size has a great influence on the particle motion characteristics. The results in this paper show that when the droplet size decreases by 50%, the particle velocity at the droplet surface increases by 7.26% to 13.85%. Thus, decreasing the droplet size can help improve the collection effect.

- (e) Simulation results show that the moving particle can affect the surrounding velocity of the gas flow field, which is ignored in the theoretical calculation. This effect becomes more apparent as the particle size increases.

6. Recommendation for Future Research

To realize the utilization of WES on marine vessels, the definition and verification of the theoretical mechanism of this technology are essential in the research in this field. The authors aim to investigate how the existence of an electrostatic field affects the behaviour of particle matter in the gas flow field around a droplet, with the ultimate objective of achieving effective control of marine diesel emissions. Additionally, implementing WES can contribute to sustainable maritime operations by significantly reducing the environmental impact of ship emissions. This technology not only promises to lower the levels of harmful pollutants but also aligns with international efforts to meet stricter emission standards. By advancing this technology, we can move closer to achieving greener shipping practices that reduce the ecological footprint of global trade.

Due to the complexity of the research topic and the time constraint, there are several things which need a further study in order to make a better analysis of the WES on particles captured before the actual application of the method.

Firstly, this study mainly focuses on the particle motion process before arriving at the droplet surface. The effect of electrostatic field on one particle movement when being captured by a droplet in a gas flow field is mainly considered in this research. However, to determine the complete process of particles captured by a droplet, the particle behaviour after arriving at the droplet surface is also crucial to identify. The particle–droplet interaction is important in the particle capturing process. Further research should focus on the interaction on the droplet surface based upon the research in this work while considering the effect of the electrostatic field.

Secondly, in this study, the motion characteristics of individual charged particles were considered in the gas flow field around the charged droplet. The charged particle moving in the gas flow field on the same axis as the charged droplet. The drag force and the electrostatic force that act on the particle are on the same vertical axis. There are no external forces in the other directions. In subsequent research, the number of particles can be increased while considering the effects between charged particles. The force analysis may be more complicated.

Finally, in the present research work, the droplet is a sphere and is considered to remain static in the gas flow field. In the theoretical model, the gas flow field distribution around the droplet is considered as the flow distribution around a sphere. But, in the practical condition, the shape of the droplet may change in the flow or because of the electrostatic field effect. Thus, there may be some differences between the theoretical results and the real-world phenomenon. Further research should take this feature into consideration.

Author Contributions: L.Y.: Conceptualization, Methodology, Software, Formal analysis, Investigation, Writing—Original Draft, Writing—Review and Editing. H.Y. and H.W.: Writing—Review and Editing. N.M. and P.Z.: Conceptualization & Supervision. All authors have read and agreed to the published version of the manuscript.

Funding: This research was funded by China Scholarship Council Foundation (CSC201906330111), High quality courses of postgraduate education, Ocean University of China (HDYK21007), Postgraduate Education Joint Cultivation Base Construction Projects, Ocean University of China (HDYJ23005).

Institutional Review Board Statement: Not applicable.

Informed Consent Statement: Not applicable.

Data Availability Statement: Data are contained within the article.

Conflicts of Interest: There are no conflicts to declare.

References

1. Corbett, J.J.; Fischbeck, P.S.; Pandis, S.N. Global Nitrogen and Sulfur Inventories for Oceangoing Ships. *J. Geophys. Res. Atmos.* **1999**, *104*, 3457–3470. [\[CrossRef\]](#)
2. Endresen, Ø.; Sørgård, E.; Sundet, J.K.; Dalsøren, S.B.; Isaksen, I.S.A.; Berglen, T.F.; Gravir, G. Emission from International Sea Transportation and Environmental Impact. *J. Geophys. Res. Atmos.* **2003**, *108*, D17. [\[CrossRef\]](#)
3. Eyring, V.; Köhler, H.W.; Van Aardenne, J.; Lauer, A. Emissions from International Shipping: 1. The Last 50 Years. *J. Geophys. Res. D Atmos.* **2005**, *110*, 171–182. [\[CrossRef\]](#)
4. Eyring, V.; Isaksen, I.S.A.; Berntsen, T.; Collins, W.J.; Corbett, J.J.; Endresen, O.; Grainger, R.G.; Moldanova, J.; Schlager, H.; Stevenson, D.S. Transport Impacts on Atmosphere and Climate: Shipping. *Atmos Environ.* **2010**, *44*, 4735–4771. [\[CrossRef\]](#)
5. Bond, T.C.; Doherty, S.J.; Fahey, D.W.; Forster, P.M.; Berntsen, T.; Deangelo, B.J.; Flanner, M.G.; Ghan, S.; Kärcher, B.; Koch, D.; et al. Bounding the Role of Black Carbon in the Climate System: A Scientific Assessment. *J. Geophys. Res. Atmos.* **2013**, *118*, 5380–5552. [\[CrossRef\]](#)
6. Eyring, V.; Stevenson, D.S.; Lauer, A.; Dentener, F.J.; Butler, T.; Collins, W.J.; Ellingsen, K.; Gauss, M.; Hauglustaine, D.A.; Isaksen, I.S.A.; et al. Multi-Model Simulations of the Impact of International Shipping on Atmospheric Chemistry and Climate in 2000 and 2030. *Atmos. Chem. Phys.* **2007**, *7*, 757–780. [\[CrossRef\]](#)
7. Di Natale, F.; Carotenuto, C. Particulate Matter in Marine Diesel Engines Exhausts: Emissions and Control Strategies. *Transp Res. D Transp. Environ.* **2015**, *40*, 166–191. [\[CrossRef\]](#)
8. Corbett, J.J.; Winebrake, J.J.; Green, E.H.; Kasibhatla, P.; Eyring, V.; Lauer, A. Mortality from Ship Emissions: A Global Assessment. *Environ. Sci. Technol.* **2007**, *41*, 8512–8518. [\[CrossRef\]](#) [\[PubMed\]](#)
9. Winebrake, J.J.; Corbett, J.J.; Green, E.H.; Lauer, A.; Eyring, V. Mitigating the Health Impacts of Pollution from Oceangoing Shipping: An Assessment of Low-Sulfur Fuel Mandates. *Environ. Sci. Technol.* **2009**, *43*, 4776–4782. [\[CrossRef\]](#)
10. Abida, H.; Moreno-Gutiérrez, J. Using Emissions of Precursor Pollutants by Ships in Different Regions to Calculate Yearly Mortality Attributable to Maritime Transport: Case for the Imo to Designate the Strait of Gibraltar an Eca Zone. *J. Appl. Sci. Environ. Stud.* **2021**, *4*, 470–481.
11. Ntziachristos, L.; Saukko, E.; Lehtoranta, K.; Rönkkö, T.; Timonen, H.; Simonen, P.; Karjalainen, P.; Keskinen, J. Particle Emissions Characterization from a Medium-Speed Marine Diesel Engine with Two Fuels at Different Sampling Conditions. *Fuel* **2016**, *186*, 456–465. [\[CrossRef\]](#)
12. Agrawal, H.; Welch, W.A.; Miller, J.W.; Cocker, D.R. Emission Measurements from a Crude Oil Tanker at Sea. *Environ. Sci. Technol.* **2008**, *42*, 7098–7103. [\[CrossRef\]](#)
13. Healy, R.M.; O'Connor, I.P.; Hellebust, S.; Allanic, A.; Sodeau, J.R.; Wenger, J.C. Characterisation of Single Particles from In-Port Ship Emissions. *Atmos. Environ.* **2009**, *43*, 6408–6414. [\[CrossRef\]](#)
14. Viana, M.; Amato, F.; Alastuey, A.; Querol, X.; Moreno, T.; Dos Santos, S.G.; Herce, M.D.; Fernández-Patier, R. Chemical Tracers of Particulate Emissions from Commercial Shipping. *Environ. Sci. Technol.* **2009**, *43*, 7472–7477. [\[CrossRef\]](#) [\[PubMed\]](#)
15. Agrawal, H.; Malloy, Q.G.J.; Welch, W.A.; Wayne Miller, J.; Cocker, D.R. In-Use Gaseous and Particulate Matter Emissions from a Modern Ocean Going Container Vessel. *Atmos. Environ.* **2008**, *42*, 5504–5510. [\[CrossRef\]](#)
16. Murphy, S.; Agrawal, H.; Sorooshian, A.; Padró, L.T.; Gates, H.; Hersey, S.; Welch, W.A.; Jung, H.; Miller, J.W.; Cocker, D.R.; et al. Comprehensive Simultaneous Shipboard and Airborne Characterization of Exhaust from a Modern Container Ship at Sea. *Environ. Sci. Technol.* **2009**, *43*, 4626–4640. [\[CrossRef\]](#)
17. Johansson, L.; Jalkanen, J.P.; Kalli, J.; Kukkonen, J. The Evolution of Shipping Emissions and the Costs of Recent and Forthcoming Emission Regulations in the Northern European Emission Control Area. *Atmos. Chem. Phys.* **2013**, *13*, 16113–16150. [\[CrossRef\]](#)
18. Lehtoranta, K.; Aakko-Saksa, P.; Murtonen, T.; Vesala, H.; Ntziachristos, L.; Rönkkö, T.; Karjalainen, P.; Kuittinen, N.; Timonen, H. Particulate Mass and Nonvolatile Particle Number Emissions from Marine Engines Using Low-Sulfur Fuels, Natural Gas, or Scrubbers. *Environ. Sci. Technol.* **2019**, *53*, 3315–3322. [\[CrossRef\]](#)
19. Sobczyk, A.T.; Jaworek, A.; Marchewicz, A.; Krupa, A.; Czech, T.; Śliwiński, Ł.; Charchalis, A. Particulate Matter Emission Reduction from Marine Diesel Engines by Electrohydrodynamic Methods. *J. KONES* **2019**, *26*, 203–210. [\[CrossRef\]](#)
20. Di Natale, F.; Carotenuto, C.; Parisi, A.; Flagiello, D.; Lancia, A. Wet Electrostatic Scrubbing for Flue Gas Treatment. *Fuel* **2022**, *325*, 124888. [\[CrossRef\]](#)
21. Sakuma, Y.; Yamagami, R.; Zukeran, A.; Ehara, Y.; Inui, T. Reduction of SO₂ and DPM Using Heat Exchanger and Electrostatic Precipitation in Diesel Engine. *Mar. Eng.* **2014**, *49*, 533–538. [\[CrossRef\]](#)
22. Carotenuto, C.; Di Natale, F.; Lancia, A. Wet Electrostatic Scrubbers for the Abatement of Submicronic Particulate. *Chem. Eng. J.* **2010**, *165*, 35–45. [\[CrossRef\]](#)
23. Ha, T.H.; Nishida, O.; Fujita, H.; Wataru, H. Enhancement of Diesel Particulate Matter Collection in an Electrostatic Water-Spraying Scrubber. *J. Mar. Sci. Technol.* **2010**, *15*, 271–279. [\[CrossRef\]](#)
24. Kojevnikova, S.; Zimmels, Y. Mechanism of collection of aerosols by an array of oppositely charged drops. *J. Aerosol Sci.* **2000**, *31*, 437–461. [\[CrossRef\]](#)
25. Kojevnikova, S.; Zimmels, Y. Mechanism of aerosol collection by two- and three-dimensional inhomogeneous arrays of charged drops. *Chem. Eng. Sci.* **2000**, *55*, 4839–4855. [\[CrossRef\]](#)
26. Zhao, H.; Zheng, C. Modeling of Gravitational Wet Scrubbers with Electrostatic Enhancement. *Chem. Eng. Technol.* **2008**, *31*, 1824–1837. [\[CrossRef\]](#)

27. Jaworek, A.; Adamiak, K.; Balachandran, W.; Krupa, A.; Castle, P.; Machowski, W. Numerical Simulation of Scavenging of Small Particles by Charged Droplets. *Aerosol Sci. Technol.* **2002**, *36*, 913–924. [[CrossRef](#)]
28. Jaworek, A.; Balachandran, W.; Krupa, A.; Kulon, J.; Lackowski, M. Wet Electroscrubbers for State of the Art Gas Cleaning. *Environ. Sci. Technol.* **2006**, *40*, 6197–6207. [[CrossRef](#)] [[PubMed](#)]
29. Krupa, A.; Jaworek, A.; Szudyga, M.; Czech, T.; Sobczyk, A.T.; Marchewicz, A.; Antes, T.; Balachandran, W.; Belega, R.; Di Natale, F.; et al. Diesel Nanoparticles Removal by Charged Spray. *Int. J. Plasma Environ. Sci. Technol.* **2016**, *10*, 2.
30. D’addio, L.; Di Natale, F.; Carotenuto, C.; Scoppa, G.; Dessy, V.; Lancia, A. Removal of fine and ultrafine combustion derived particles in a wet electrostatic scrubber. In Proceedings of the XXXVI Meeting of the Italian Section of the Combust, Naples, Italy, 13–15 June 2013.
31. Di Natale, F.; Carotenuto, C.; D’Addio, L.; Jaworek, A.; Krupa, A.; Szudyga, M.; Lancia, A. Capture of Fine and Ultrafine Particles in a Wet Electrostatic Scrubber. *J. Environ. Chem. Eng.* **2015**, *3*, 349–356. [[CrossRef](#)]
32. Prasad, R.; Bella, V.R. A Review on Diesel Soot Emission, Its Effect and Control. *Bull. Chem. React. Eng. Catal.* **2010**, *5*, 69–86. [[CrossRef](#)]
33. Matti Maricq, M. Chemical Characterization of Particulate Emissions from Diesel Engines: A Review. *J. Aerosol Sci.* **2007**, *38*, 1079–1118. [[CrossRef](#)]
34. Burtscher, H. Physical Characterization of Particulate Emissions from Diesel Engines: A Review. *J. Aerosol Sci.* **2005**, *36*, 896–932. [[CrossRef](#)]
35. Zhou, S.; Zhou, J.; Feng, Y.; Zhu, Y. Marine Emission Pollution Abatement Using Ozone Oxidation by a Wet Scrubbing Method. *Ind. Eng. Chem. Res.* **2016**, *55*, 5825–5831. [[CrossRef](#)]
36. Zhou, S.; Zhou, J.; Zhu, Y. Chemical Composition and Size Distribution of Particulate Matters from Marine Diesel Engines with Different Fuel Oils. *Fuel* **2019**, *235*, 972–983. [[CrossRef](#)]
37. Cha, C.Y.; McCoy, B.J. Thermal Force on Aerosol Particles. *Phys. Fluids* **1974**, *17*, 1376–1380. [[CrossRef](#)]
38. Jaworek, A.; Krupa, A.; Sobczyk, A.T.; Marchewicz, A.; Szudyga, M.; Antes, T.; Balachandran, W.; Di Natale, F.; Carotenuto, C. Submicron Particles Removal by Charged Sprays. Fundamentals. *J. Electrostat.* **2013**, *71*, 345–350. [[CrossRef](#)]
39. D’Addio, L.; Di Natale, F.; Carotenuto, C.; Balachandran, W.; Lancia, A. A Lab-Scale System to Study Submicron Particles Removal in Wet Electrostatic Scrubbers. *Chem. Eng. Sci.* **2013**, *97*, 176–185. [[CrossRef](#)]
40. Rayleigh, L. XX. On the Equilibrium of Liquid Conducting Masses Charged with Electricity. *Lond. Edinb. Dublin Philos. Mag. J. Sci.* **1882**, *14*, 184–186. [[CrossRef](#)]

Disclaimer/Publisher’s Note: The statements, opinions and data contained in all publications are solely those of the individual author(s) and contributor(s) and not of MDPI and/or the editor(s). MDPI and/or the editor(s) disclaim responsibility for any injury to people or property resulting from any ideas, methods, instructions or products referred to in the content.